Nanoscale Advances

ROYAL SOCIETY OF CHEMISTRY

PAPER

View Article Online
View Journal | View Issue

Cite this: *Nanoscale Adv.*, 2022, **4**, 1808

Development of S4A–BSA–Au NPs for enhanced anti-tumor therapy of canine breast cancer†

Qi Chen, ‡[ab] Chengfang Xu,‡[ab] Zhonghao Sun,‡[c] Jingjing Yang,[d] Fan Chen,[d] Zixiang Lin,[a] Degui Lin,[a] Yanyan Jiang *[d] and Jiahao Lin*[ab]

S4A ((1*R*,2*R*,3*S*)-1,2-propanediol acetal-zeylenone) is one of the derivatives of zeylenone and exhibits superior cytotoxicity against the canine breast cancer cell line CIPp. However, its poor aqueous solubility and toxicity to normal tissue limit its clinical application. Therefore, in order to enhance the anticancer effect of S4A, in this article, BSA/BSA–Au-nanocluster-aggregated core/shell nanoparticles (B-BANC-NPs) were prepared by using bovine serum albumin (BSA) and $HAuCl_4$, and then we further synthesized S4A–BSA–Au NPs which were spherical, with a diameter of about 60 nm. *In vitro* cytotoxicity assessed by using CCK-8 assay demonstrated that the IC_{50} value of the S4A–BSA–Au NPs was 10.39 μg mL^{-1}, which was not significantly different from that of S4A (10.45 μg mL^{-1}). *In vitro* apoptosis assay showed that the apoptosis rate of cells treated with S4A–BSA–Au NPs was 20.12%, which was significantly higher than that of the control group treated with S4A (11.3%). Notably, S4A–BSA–Au NPs were shown to effectively accumulate at tumor sites with fluorescence tracing. Besides, the effect of S4A–BSA–Au NPs on SPARC expression was determined by western blotting, and the result showed that 24 h after applying S4A–BSA–Au NPs, SPARC expression in low, middle and high dosage groups was lower than that of the control group, and the tendency showed dose dependence. The results revealed that S4A–BSA–Au NPs could effectively improve the anti-tumor activity of S4A on canine breast cancer, which may be associated with their abilities to effectively accumulate within tumor and to reduce the expression of SPARC.

Received 22nd August 2021
Accepted 16th October 2021

DOI: 10.1039/d1na00640a

rsc.li/nanoscale-advances

1. Introduction

Among all neoplasms, canine breast cancer is the most common form of cancer in female dogs.[1] At present, surgical excision is regarded as the best method to treat it. However, surgery is not suitable for all dogs due to extensive tumor invasion and high incidence of distant metastases.[2] Besides, despite treatment, the survival rate is low. Studies have shown that surgical resection combined with chemotherapy can reduce the recurrence rate and improve the survival rate.[3] However, the efficacy of chemotherapy may be limited by the possibility of developing drug resistance, which depends critically on the sensitivity of tumor cells to chemotherapy drugs.[4,5]

Zeylenone (Zey) is a natural cyclohexene oxide compound isolated from *Uvaria grandiflora* Roxb.[6] Since the discovery of Zey in 1997, researchers have carried out multiple studies on its manufacturing processes (synthesis/semi-synthesis), pharmacodynamics, molecular mechanism, *etc.*, and it was considered to be an anti-tumor drug candidate with great potential.[7–10] Studies have shown that Zey could induce significant cell apoptosis through a mitochondrial apoptosis pathway and inhibit the invasion and migration of gastric cancer cells.[11] Furthermore, it was reported that Zey had significant inhibitory activity against a variety of tumor cells, which was time-dependent and dose-dependent, and its anti-tumor activity was similar to that of paclitaxel.[12] However, the formulation development of Zey is an urgent problem to be solved because of its low water solubility and poor stability.

Gold nanoclusters (Au NCs), consisting of a few to hundreds of atoms,[13] have been widely applied as fluorescent probes. Their fluorescence spectrum can be tuned to peak in the visible and near infrared region due to their particular size effect. Such fluorescence characteristics give them great potential to be applied in biological imaging and detection.[14–16] Derived from Au NCs, albumin-stabilized Au NCs can not only retain the

[a]*College of Veterinary Medicine, China Agricultural University, No. 2, Yuanmingyuan West Road, Haidian District, Beijing, China. E-mail: jiahao_lin@cau.edu.cn*

[b]*Center of Research and Innovation of Chinese Traditional Veterinary Medicine, China*

[c]*Institute of Medicinal Biotechnology, Chinese Academy of Medical Sciences, Peking Union Medical College, Beijing 100730, China*

[d]*Key Laboratory for Liquid-Solid Structural Evolution and Processing of Materials, Ministry of Education, Shandong University, Jinan 250061, China. E-mail: yanyan.jiang@sdu.edu.cn*

† Electronic supplementary information (ESI) available. See DOI: 10.1039/d1na00640a

‡ These authors contributed equally to this work and should be considered co-first authors.

original excellent properties of Au NCs, but also increase the drug stability benefited by their core–shell structure.

Although Au NCs give drugs fluorescence imaging properties *in vivo*, approaches are urgently needed to achieve their targeting efficiency. Fortunately, in addition to passively delivering nano-drugs to tumor sites through EPR effects,[17] the targeting of these drugs can be further enhanced by binding with albumin.[18] SPARC is a protein found to be over-expressed on human breast cancer cells,[19] and shows high binding affinity to albumin.[20] The affinity between albumin and SPARC enables albumin-bound drugs to specifically target breast tumor, leading to higher drug accumulation within the tumor focus.

A previous study of Zey and its 13 derivatives in our laboratory indicated that S4A (Fig. S1†) exhibited a strong cytotoxic effect against the canine breast cancer cell line CIPp, with a higher yield and solubility. Therefore, we selected S4A for the subsequent anti-tumor studies. In order to improve the solubility and enhance the targeting properties of S4A, we synthesized S4A–BSA–Au NPs (Fig. 1). Then, their anti-tumor effect was further verified through a cytotoxicity test and pro-apoptotic study. While the accumulation effect on canine breast cancer focus was evaluated by fluorescence tracing in tumor-bearing mice, and its mechanism was further explored from the expression level of SPARC on the canine breast cancer cell line. Through the above investigations, we hope to prove the anti-tumor effect of S4A by using the drug delivery system B-BANC-NPs, to provide a basis for the pharmaceutical improvement strategy of hydrophobic natural products and new dosage forms for canine breast cancer treatment.

2. Materials and methods

2.1 Chemicals and reagents

S4A was synthesized and kindly provided by the Institute of Medicinal Plant Development, Chinese Academy of Medical Sciences & Peking Union Medical College (Beijing, China). Fetal bovine serum (FBS), DMEM and 0.25% (w/v) trypsin–EDTA solution were purchased from Gibco (America). Dimethyl sulphoxide (DMSO) was provided by Sigma (Spain). Penicillin–streptomycin was obtained from Hyclone (America). Tris–HCl was obtained from Beijing Solarbio Science & Technology Co., Ltd. (Beijing, China). The marker (10–180 kDa) and loading-buffer (6×) were purchased from Beijing Transgen Biotech Co. Ltd. (Beijing, China). The first antibody against SPARC was purchased from Abcam (Shanghai, China) and that against α-tubulin was purchased from CST (Shanghai, China). Goat anti-rabbit IgG (H + L) was obtained from Biolab (Beijing, China). Gold(III) chloride trihydrate ($HAuCl_4 \cdot 3H_2O$) and bovine serum albumin (BSA) were purchased from Shanghai Macklin Biochemical Co., Ltd. (Shanghai, China).

2.2 Preparation and characterization

2.2.1 Preparation of BSA-stabilized Au NCs. 10 mL aqueous solution of $HAuCl_4$ (10 mM) was added into 10 mL aqueous solution of BSA (50 mg mL^{-1}) at 37 °C under vigorous stirring. After 2 min, 1 mL NaOH (1 M) was added to adjust the pH value of the solution to 12. Then, the mixture was stabilized under vigorous stirring for 1 h at 70 °C. The color of the mixture changed into brown from light yellow, indicating the formation of BSA-stabilized Au NCs. Finally, the mixture was purified using a dialysis bag (MW: 8000–14 000 Da) for 24 h, and the ultrapure water was totally changed every 3 to 4 h to remove excess ions.

2.2.2 Preparation of B-BANC-NPs and S4A–BSA–Au NPs. 1 mL BSA solution (50 mg mL^{-1}) was added into 4 mL purified Au NC solution (containing about 50 mg BSA) under stirring at a speed of 200 rpm for 2 min. Then, 50 μL S4A (20 mg mL^{-1}) was added into the mixture under stirring at 750 rpm, and the mixture was stabilized for 3 h. After that, 3 mL ethanol was added into the solution mixture with an injection pump at a rate of 1 mL min^{-1}. The reaction was allowed to stir for 2 h at room temperature. Finally, the product was transferred into a dialysis

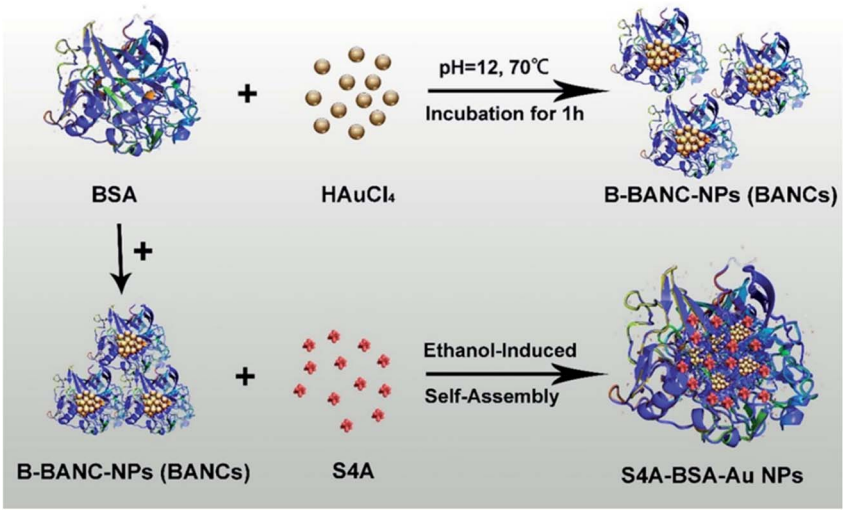

Fig. 1 S4A–BSA–Au NPs were prepared by ethanol-induced self-assembly with BSA and B-BANC-NPs (BANCs) as precursors achieving an excellent anticancer effect after loading with S4A.

bag (MWCO: 8000–14 000 Da) and dialyzed against ultrapure water for 24 h. Water was changed every 3 to 4 h to remove ethanol. The process of the preparation of B-BANC-NPs was similar to the above without the addition procedure of S4A.

2.2.3 Characterization. The morphology and size of the B-BANC-NPs and S4A–BSA–Au NPs were determined by transmission electron microscopy (TEM). The hydrodynamic diameter, size distribution (polydispersity index, PDI) and zeta potential of the samples were measured by using a Zetasizer Nano ZS. The drug loading content (LC) and encapsulated efficiency (EE) of S4A–BSA–Au NPs were confirmed *via* a UV-vis spectrophotometer.

2.3 *In vitro* study

2.3.1 Cell culture. The canine breast cancer cell line CIPp was donated by the University of Tokyo (Tokyo, Japan). The CIPp cells were cultured in Dulbecco's Modified Eagle's Medium (DMEM), and supplemented with 10% fetal bovine serum (FBS) and 100 U antibiotics (streptomycin and penicillin) at 37 °C in a humid environment gassed with 5% CO_2.

2.3.2 Cytotoxicity of S4A–BSA–Au NPs. CIPp cells in the logarithmic growth phase were collected, and then seeded into 96-well plates (5000 cells per well) and incubated for 24 h. Then, 100 μL S4A–BSA–Au NPs at various concentrations were added respectively when the cells sticked to the wall and fused to 70–90%. After 24 h, 90 μL DMEM and 10 μL enhanced CCK-8 reagent were added into each well, and incubated for 30 min in the dark. Finally, the OD value was measured by using a microplate reader. Each experiment was performed in triplicate.

2.3.3 Pro-apoptotic effect of S4A–BSA–Au NPs. Annexin V and FITC mixtures were used to evaluate the apoptosis induction ability of S4A and S4A–BSA–Au NPs. Following the treatment with S4A and S4A–BSA–Au NPs at a concentration of 15 μg mL^{-1} for 24 h, the cell suspension was diluted with 400 μL 1× binding buffer and strained through a 300-mesh sieve. Then, 5 μL Annexin V and FITC mixtures were added followed by flow cytometric analysis.

2.3.4 Western blotting. The cells were treated with normal saline and S4A–BSA–Au NPs at various concentrations and divided into 4 groups, which were the normal saline group (C) 200 μL, low concentration group (L) 0.1 mg μL^{-1}, medium concentration group (M) 0.15 mg μL^{-1} and high concentration group (H) 0.2 mg μL^{-1}. After 24 h, each group was rinsed twice with precooled PBS, and 250 μL RIPA lysis buffer (with 1% PMSF) was added to each well. The cells were collected after being placed in a fridge at 4 °C for 30 min, and gently blown with a transfer liquid gun to avoid bubbles. Ultrasonic cracking was performed when the sample was still viscous. Each sample was decomposed for 10 to 15 s until it became clear liquid and could flow freely. Then, loading buffer (6×) was added into each EP tube and the sample was placed in a boiling water bath for more than 5 min. The processed sample was stored at −20 °C, and proteins were transferred by electrophoresis onto PVDF membranes. Then, the membranes were blocked with 5% non-fat milk and subsequently incubated with primary antibodies at 37 °C overnight, prior to the incubation with secondary antibodies for 90 min. Finally, protein bands were detected by enhanced chemiluminescence.

2.4 *In vivo* studies

2.4.1 Animals and breast tumor xenograft model. 20 female Balb/C nude mice (SPF grade, 5 weeks old) weighing 12–14 g, purchased from Beijing Vital River Laboratory Animal Technology Co., Ltd. (Beijing, China), were used in this study. They were acclimated to the animal facility for 3 days before conducting this experiment. The right breast areas of these mice were subcutaneously implanted with 1×10^7 CIPp cells. After the tumor grew to reach about a volume of 300–500 mm^3, the mice were randomized into 4 groups with peritumoral/intratumoral injection as the administration route (control group (C): 200 μL normal saline, low concentration group (L): 0.1 mg μL^{-1} S4A–BSA–Au NPs, moderate concentration group (M): 0.15 mg μL^{-1} S4A–BSA–Au NPs, and high concentration group (H): 0.2 mg μL^{-1} S4A–BSA–Au NPs). All animal studies were conducted in accordance with the protocols of the Animal

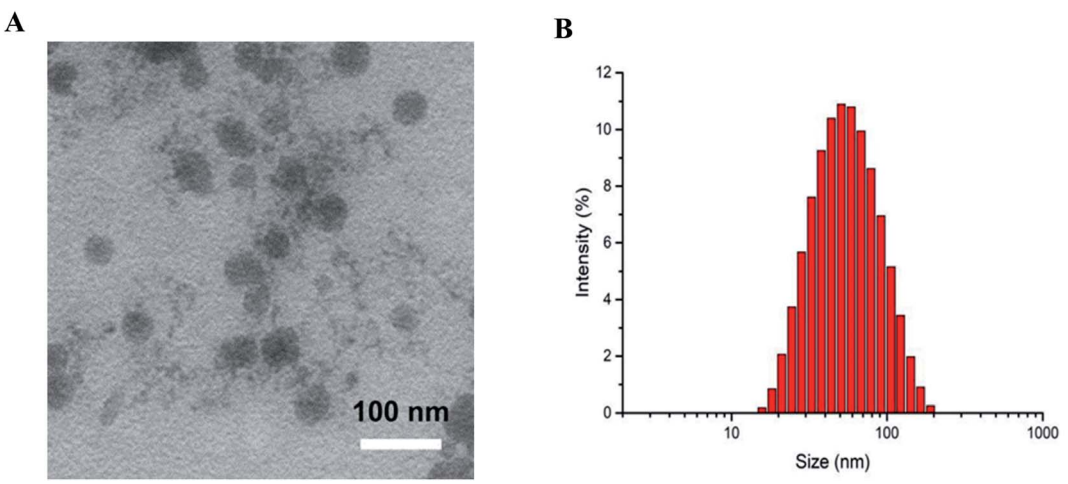

Fig. 2 (A) TEM image of B-BANC-NPs (bar = 100 nm). (B) Size distribution of B-BANC-NPs measured by the DLS technique.

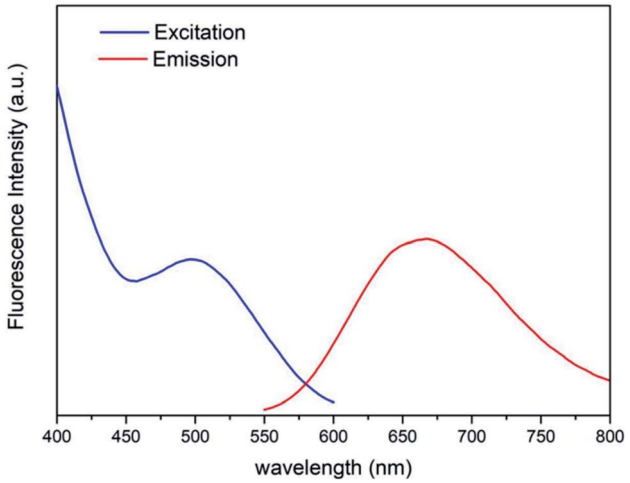

Fig. 3 Excitation section spectra with λ_{em} = 675 nm and emission spectra with λ_{ex} = 495 nm of B-BANC-NP solution.

Management Rules of the Ministry of Health of the People's Republic of China (document no. 55, 2001) and were approved by the China Agricultural University Laboratory Animal Welfare and Animal Experimental Ethical Committee (Beijing, China).

2.4.2 Fluorescence tracing *in vivo*. After administration, the mice were scanned at 6 h, 12 h and 24 h using an IVIS® Spectrum imaging system, with the excitation wavelength set at 580 nm and emission at 630 nm. At 24 h, the tumors were excised, and their fluorescence intensities were measured.

2.5 Statistical analysis

Comparisons between groups were performed using ANOVA (Prism GraphPad 7 Software).

3. Results

3.1 Characterization

In order to improve the efficiency of S4A delivery to canine breast tumor, SPARC-mediated targeting is a promising approach to achieve tumor-specific delivery after systemic administration. Therefore, in this research, we initially synthesized B-BANC-NPs as the delivery system of S4A by ethanol-induced self-assembly nanotechnology. As shown in Fig. 2A, the spherical morphology of B-BANC-NPs was determined by transmission electron microscopy (TEM) with a diameter of about 44 nm. The size distribution of B-BANC-NPs was obtained by dynamic light scattering (DLS) as shown in Fig. 2B. The mean diameter of B-BANC-NPs was 47.16 nm (*Z*-average), with a polydispersity index (PDI) of 0.243. The result was suitable for TEM, indicating that B-BANC-NPs were successfully synthesized. The surface charge of the nanoparticles was also measured to be −22.1 mV, which was consistent with the surface charge of the protein under a neutral environment, suggesting that there is an intact BSA corona outside the spherical nanoparticle to keep it stable in aqueous solution.

The fluorescence properties of the B-BANC-NP solution were measured by fluorescence spectroscopy (Fig. 3). The maximum excitation and emission were found to be 495 nm and 675 nm,

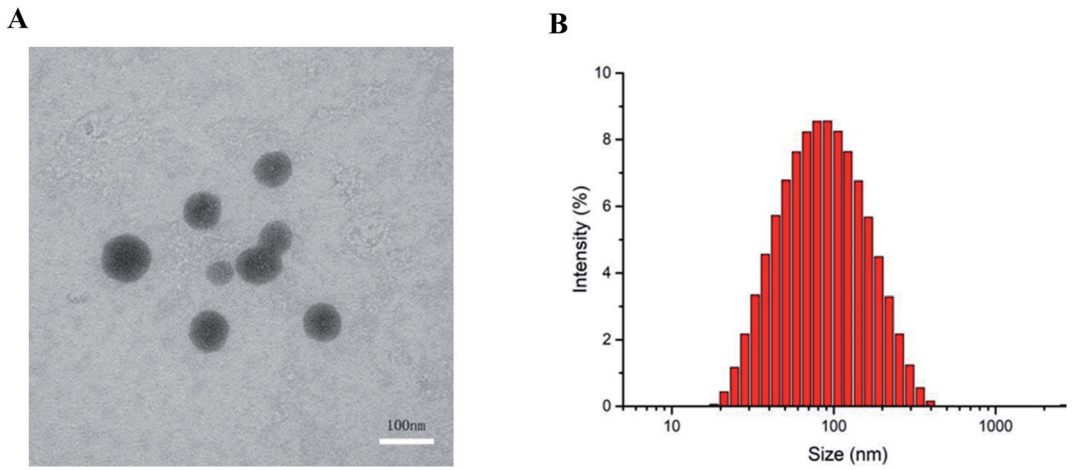

Fig. 4 (A) TEM image of S4A–BSA–Au NPs (bar = 100 nm). (B) Size distribution of S4A–BSA–Au NPs measured by the DLS technique.

Table 1 Particle diameter, mean diameter, PDI and zeta potential of B-BANC-NPs and S4A–BSA–Au NPs

Sample	Particle diameter[a] (nm)	Mean diameter[b] (nm)	PDI[b]	Zeta potential[b] (mV)
B-BANC-NPs	44	47.16	0.243	−22.1
S4A–BSA–Au NPs	60	73.10	0.342	−22.8

[a] Particle diameter measured by TEM. [b] Mean diameter, polydispersity index (PDI) of particle distribution and zeta potential measured by dynamic light scattering (DLS).

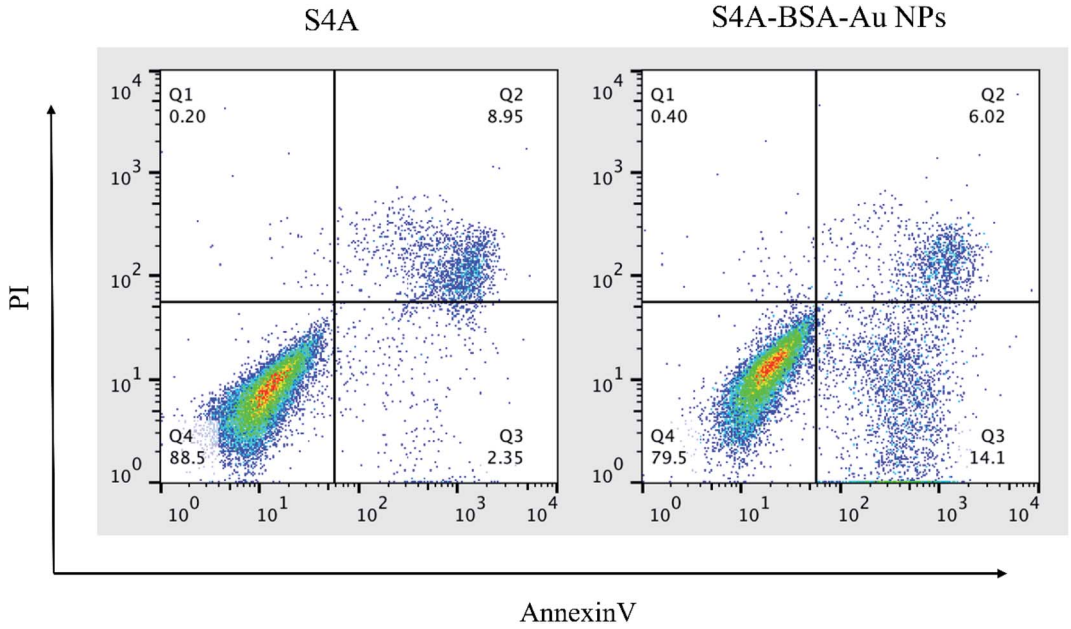

Fig. 5 Effect of the S4A group and S4A–BSA–Au NP group on apoptosis in the CIPp cell line.

respectively. And the innate fluorescence derived from the Au NCs could be applied as a fluorescent probe in our following investigations.

The TEM image of S4A–BSA–Au NPs in Fig. 4A indicated that the spherical nanoparticles have an average size of about 60 nm. The result was consistent with that of the DLS analysis, which showed that the average diameter of S4A–BSA–Au NPs was about 73.10 nm with a PDI of 0.342 in water (Fig. 4B). The particle size increased after the loading of S4A. The surface charge of S4A–BSA–Au NPs was −22.8 mV (Table 1).

S4A was loaded into nanoparticles by diffusion absorption and hydrophobic-induced self-assembly embedding with hydrophobic characters. After the synthesis of S4A–BSA–Au NPs, the encapsulation efficiency and drug loading efficiency measured *via* spectrophotometry were 70.52% and 0.71%, respectively.

3.2 *In vitro* anti-tumor activity

The anti-tumor activity of S4A and S4A–BSA–Au NPs was evaluated from their IC_{50} value and ability to induce apoptosis against the CIPp cell line. The IC_{50} value of the S4A–BSA–Au NPs was 10.39 μg mL^{-1}, which was not significantly different from that of S4A (10.45 μg mL^{-1}) for the CIPp cell line. The result revealed that the cytotoxicity of S4A–BSA–Au NPs on CIPp cells was similar to that of S4A. Nevertheless, the result of the apoptosis rate indicated that the total percent of apoptotic cells treated with S4A–BSA–Au NPs was 20.12%, which was significantly higher than that of the S4A treated group (11.3%) (Fig. 5).

3.3 *In vivo* imaging in tumor-bearing mice

To determine the tumor accumulation ability of S4A–BSA–Au NPs, a fluorescence tracing experiment *in vivo* was performed. Fig. 6 shows the distribution state of S4A–BSA–Au NPs in real time and their accumulation in tumor with different concentrations (0.1 to 0.2 mg μL^{-1}). The results at three time points all revealed that the fluorescence signal of group L was the weakest, followed by group M, and that of group H was the strongest. The liver showed a strong fluorescent signal 6 h after administration with S4A–BSA–Au NPs. With the passage of time, the signal in the liver gradually weakened. At 24 h, there was no obvious

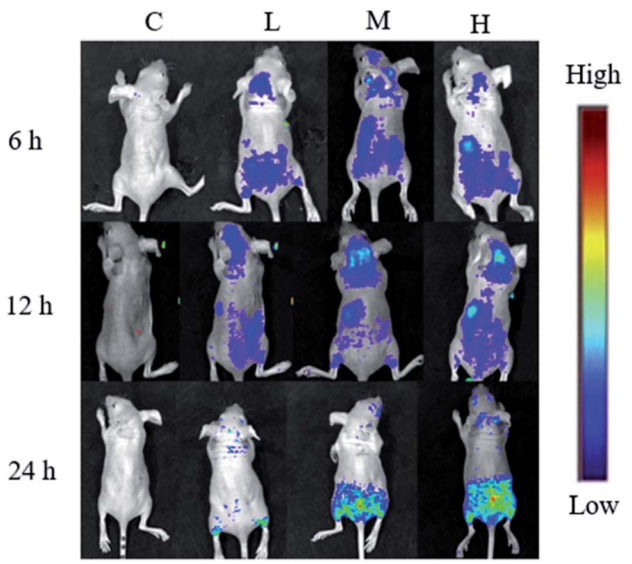

Fig. 6 *In vivo* non-invasive NIRF images of time-dependent imaging of CIPp tumor-bearing mice after peritumoral/intratumoral injection of S4A–BSA–Au NPs with different concentrations (control group (C): 200 μL normal saline, low concentration group (L): 0.1 mg μL^{-1}, moderate concentration group (M): 0.15 mg μL^{-1}, and high concentration group (H): 0.2 mg μL^{-1}).

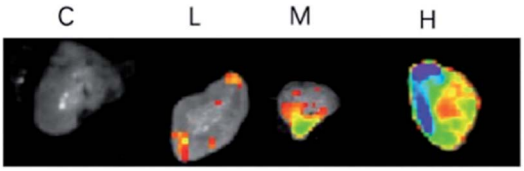

Fig. 7 The *ex vivo* optical images of tumors of CIPp tumor-bearing mice sacrificed 24 h after the peritumoral/intratumoral injection of S4A–BSA–Au NPs.

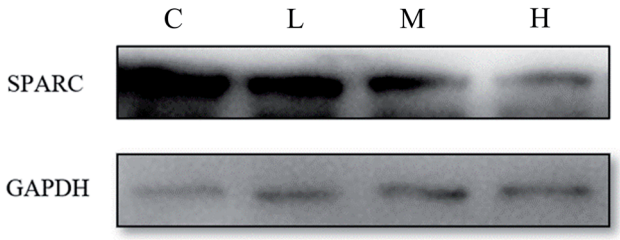

Fig. 8 Expression of SPARC protein on the CIPp cells of canine breast tumor.

fluorescence signal in both brain tissue and liver tissue, while the signal in the hindquarter was the strongest, which was consistent with the tumor site.

At 24 h, the tumors of mice were separated, and as shown in Fig. 7, there was no fluorescence signal in the tumor of group C. In contrast, groups L, M, and H displayed obvious fluorescence signals, and the signal in group H was the strongest, followed by group M, and that of group L was the weakest, which was consistent with the result of real-time distribution.

3.4 Effect of S4A–BSA–Au NPs on SPARC expression

The effect of S4A–BSA–Au NPs with different concentrations (0.1 to 0.2 mg μL^{-1}) on SPARC expression was assessed by western blotting. According to Fig. 8, the expression level of SPARC was ranked as follows: group C, group L, group M, and group H. Furthermore, the expression level of SPARC in group L, group M and group H was lower than that of the control group, and decreased in a dose dependent manner.

4. Discussion

Although S4A exhibits promising anticancer activity, its clinical practice and therapeutic effect are limited by the poor hydrophilicity. Therefore, it is necessary to put forward solutions. Albumin possesses the advantages of good biocompatibility, biodegradability and hydrophilicity, and can be administered intravenously.[16] Through non-covalent association with albumin, the solubility of hydrophobic drugs can be increased.[21] In this study, we successfully synthesized S4A–BSA–Au NPs using bovine serum albumin, which can improve the poor solubility of S4A to a great extent, realize intravenous administration of S4A, and achieve a better therapeutic effect at the same concentration. When the size of B-BANC-NPs and S4A–BSA–Au NPs was measured by DLS and TEM respectively, the particle size determined by TEM seems relatively less than that of DLS, which is likely due to the fact that the particles aggregate together and they are surrounded by water in DLS measurements, while TEM just measures the single particle in the vacuum environment.

Au NCs, with a particle diameter less than 2 nm, exhibit unique size effects and distinct fluorescence characteristics. Recently, BSA has often been used in the synthesis of Au NCs, because albumin-stabilized Au NCs are more biocompatible and photostable.[22] Nanoparticle albumin-bound (nab) paclitaxel (nab-paclitaxel; Abraxane) has been approved in 2006 for use in patients with metastatic breast cancer who have failed in combination chemotherapy.[23] Inspired by nab-technology, we used native BSA and BSA-stabilized Au NCs to synthesize S4A–BSA–Au NPs in this study. The as-prepared drug carriers inherit the properties of nab-paclitaxel which can have an actively targeting capacity towards tumors. Besides, Au NCs possess superior optical properties, which could be applied for developing a promising bioimaging platform.[24,25] Therefore, embedded BSA-stabilized Au NCs were prepared to make this drug delivery system traceable *in vivo*.

In vivo fluorescence tracing experiment, signal could be consistently detected in tumor tissue of mice within 24 hours. The result suggests that S4A–BSA–Au NPs show superior accumulation and promising retention behavior in tumor sites, which might be partly due to the dysplasia of vascular wall and lymphatic obstruction,[26] and also partly because S4A–BSA–Au NPs are prepared from BSA. Albumin is a versatile drug carrier in anti-cancer drug delivery systems and it also has an actively targeting capacity towards tumors. Because solid tumors require a large number of amino acids which are mainly provided by albumin during their growth.[27] And albumin was reported to be transported into the tumor *via* a specific transport mechanism (gp60-caveolin-1-SPARC),[28] which means that S4A–BSA–Au NPs prepared by using BSA as the raw carrier material can possibly utilize this unique transport pathway of albumin to achieve the active targeting effect, and ultimately increase the accumulation of S4A on tumor focus.

The high expression level of SPARC is generally related to the poor prognosis of breast tumor.[29,30] In our study, we found that the expression of SPARC decreased after administration with S4A–BSA–Au NPs in a dose-dependent manner. Studies have shown that albumin could be transported into the tumor *via* a SPARC-mediated transport mechanism. Reduced expression of SPARC protein means less albumin is available for tumor growth, which may be another reason why S4A–BSA–Au NPs can enhance the anticancer effect of S4A.

5. Conclusion

In the present study, we have successfully prepared S4A–BSA–Au NPs to deliver S4A to canine breast tumor effectively. They showed a significantly higher cell apoptosis rate than S4A and could effectively reduce the clinical dosage of S4A. Notably, S4A–BSA–Au NPs also showed credible accumulation ability in canine breast tumor and could significantly reduce the expression of SPARC. Taken together, the result revealed that S4A–

BSA–Au NPs exhibited great potential in the treatment of canine breast cancer. Therefore, the drug delivery system B-BANC-NPs we proposed herein might offer a new strategy for pharmaceutical improvement of hydrophobic natural medicine.

Author contribution

Qi Chen: formal analysis, writing – original draft, writing – review and editing. Chengfang Xu: experimental conduction and visualization. Zhonghao Sun: resources. Jingjing Yang: experimental conduction, visualization, and writing – review. Fan Chen: experimental conduction. Zixiang Lin: experimental conduction. Degui Lin: resources. Yanyan Jiang: data curation, writing – review, and funding acquisition. Jiahao Lin: conceptualization, data curation, writing – review, and funding acquisition.

Conflicts of interest

The authors declare no conflict of interest.

Acknowledgements

We greatly acknowledge financial support from the National Natural Science Foundation of China (Grant no. 31972730), the 2115 Talent Development Program of China Agricultural University (Grant no. 00109023), the Natural Science Foundation of Shandong Province (ZR2019BEM024), the Shenzhen Fundamental Research Program (JCYJ20190807092803583), and the Natural Science Foundation of Jiangsu Province (Grant No. BK20190205). And we are grateful to the Institute of Medicinal Plant Development (IMPLAD) for kindly providing the compound S4A.

References

1 B. G. Giovanni, G. Andrea, M. Valentina, Z. Valentina, P. Ilaria, B. Chiara, P. Salvatore, P. Marta and A. Elisabetta, *Animals*, 2020, **10**, 1687.
2 K. U. Sorenmo, R. Rasotto, V. Zappulli and M. H. Goldschmidt, *Vet. Pathol.*, 2011, **48**, 85–97.
3 M. Fatum, E. McVeigh and T. Child, *Hum. Fertil.*, 2013, **16**, 235–240.
4 K. Hida, H. Kikuchi, N. Maishi and Y. Hida, *Cancer Lett.*, 2017, **400**, 305–310.
5 M. Riesco-Martinez, K. Parra, R. Saluja, G. Francia and U. Emmenegger, *Cancer Lett.*, 2017, **400**, 311–318.
6 X. Xu, J. Shi, H. Gao and Q. Li, *J. Obstet. Gynaecol. Res.*, 2018, **44**, 1451–1457.
7 Z. Yi, L. An, Y. Z. Guang, L. Jia, X. L. Zhen and Y. S. Lin, *Chem. Pharm. Bull.*, 2006, **54**, 1459–1461.
8 L. Theerachart, S. Patchreenart, C. Kittipong and D. Tanwawan, *Acta Crystallogr., Sect. E: Crystallogr. Commun.*, 2020, **76**, 1096–1100.
9 S. Zeng, B. Zhu, J. Zeng, W. Wu and C. Jiang, *Mol. Med. Rep.*, 2018, **18**, 5572–5578.
10 X. Hu, R. Han, L. Quan, C. Liu and Y. Liao, *Int. J. Pharm.*, 2013, **450**, 331–337.
11 S. Yang, Y. Liao, L. Li, X. Xu and L. Cao, *Molecules*, 2018, **23**, 2149.
12 L. Zhang, J. Jin, L. Zhang, R. Hu, L. Gao, X. Huo, D. Liu, X. Ma, C. Wang, J. Han, L. Li, X. Sun and L. Cao, *J. Proteomics*, 2015, **126**, 279–287.
13 J. Zheng, P. R. Nicovich and R. M. Dickson, *Annu. Rev. Phys. Chem.*, 2007, **58**, 409–431.
14 P. Sharma, S. C. Brown, N. Bengtsson, Q. Zhang, G. A. Walter, S. R. Grobmyer, S. Santra, H. Jiang, E. W. Scott and B. M. Moudgil, *Chem. Mater.*, 2008, **20**, 6087–6094.
15 S. Xu, Y. Nie, L. Jiang, J. Wang, G. Xu, W. Wang and X. Luo, *Anal. Chem.*, 2018, **90**, 4039–4045.
16 J. Wang and B. Zhang, *Curr. Med. Chem.*, 2018, **25**, 2938–2953.
17 A. Bunker, A. Magarkar and T. Viitala, *Biochim. Biophys. Acta*, 2016, **1858**, 2334–2352.
18 G. Sanità, P. Armanetti, B. Silvestri, B. Carrese, G. Calì, G. Pota, A. Pezzella, M. D'Ischia, G. Luciani, L. Menichetti and A. Lamberti, *Front. Bioeng. Biotechnol.*, 2020, **8**, 765.
19 J. Feng and L. Tang, *Curr. Pharm. Des.*, 2014, **20**, 6182–6190.
20 I. T. Tai and M. J. Tang, *Drug Resist. Updates*, 2008, **11**, 231–246.
21 L. Noorani, M. Stenzel, R. Liang, M. H. Pourgholami and D. L. Morris, *J. Nanobiotechnol.*, 2015, **13**, 25.
22 L. Dong, M. Li, S. Zhang, J. Li, G. Shen, Y. Tu, J. Zhu and J. Tao, *Small*, 2015, **11**, 2571–2581.
23 W. J. Gradishar, *Expert Opin. Pharmacother.*, 2006, **7**, 1041–1053.
24 L. Qinzhen, P. Yiting, C. Tiankai, Y. Du, G. Honghua, Z. Buchang, X. Jianping, Y. Haizhu and Z. Manzhou, *Nanoscale*, 2018, **10**, 10166–10172.
25 Y. Zheng, L. Lai, W. Liu, H. Jiang and X. Wang, *Adv. Colloid Interface Sci.*, 2017, **242**, 1–16.
26 S. H. Kiaie, S. Mojarad-Jabali, F. Khaleseh, S. Allahyari, E. Taheri, P. Zakeri-Milani and H. Valizadeh, *Int. J. Pharm.*, 2020, **581**, 119269.
27 G. Stehle, H. Sinn, A. Wunder, H. H. Schrenk, J. C. Stewart, G. Hartung, W. Maier-Borst and D. L. Heene, *Crit. Rev. Oncol. Hematol.*, 1997, **26**, 77–100.
28 N. Desai, V. Trieu, B. Damascelli and P. Soon-Shiong, *Transl. Oncol.*, 2009, **2**, 59–64.
29 G. Watkins, A. Douglas-Jones, R. Bryce, R. E. Mansel and W. G. Jiang, *Prostaglandins, Leukotrienes Essent. Fatty Acids*, 2005, **72**, 267–272.
30 J. Ma, S. Gao, X. Xie, E. Sun, M. Zhang, Q. Zhou and C. Lu, *Oncol. Lett.*, 2017, **14**, 5876–5882.